DESY 95-108
hep-ex/9506012
June 1995

ISSN 0418-9833

Transverse Energy and Forward Jet Production in the Low x Regime at HERA

H1 Collaboration

Abstract

The production of transverse energy in deep inelastic scattering is measured as a function of the kinematic variables x and Q^2 using the H1 detector at the ep collider HERA. The results are compared to the different predictions based upon two alternative QCD evolution equations, namely the Dokshitzer-Gribov-Lipatov-Altarelli-Parisi (DGLAP) and the Balitsky-Fadin-Kuraev-Lipatov (BFKL) equations. In a pseudorapidity interval which is central in the hadronic centre of mass system between the current and the proton remnant fragmentation region the produced transverse energy increases with decreasing x for constant Q^2 . Such a behaviour can be explained with a QCD calculation based upon the BFKL ansatz. The rate of forward jets, proposed as a signature for BFKL dynamics, has been measured.

to be submitted to Phys. Lett.

H1 Collaboration

S. Aid[13], V. Andreev[25], B. Andrieu[28], R.-D. Appuhn[11], M. Arpagaus[36], A. Babaev[24], J. Bähr[35], J. Bán[17], Y. Ban[27], P. Baranov[25], E. Barrelet[29], R. Barschke[11], W. Bartel[11], M. Barth[4], U. Bassler[29], H.P. Beck[37], H.-J. Behrend[11], A. Belousov[25], Ch. Berger[1], G. Bernardi[29], R. Bernet[36], G. Bertrand-Coremans[4], M. Besançon[9], R. Beyer[11], P. Biddulph[22], P. Bispham[22], J.C. Bizot[27], V. Blobel[13], K. Borras[8], F. Botterweck[4], V. Boudry[7], A. Braemer[14], F. Brasse[11], W. Braunschweig[1], V. Brisson[27], D. Bruncko[17], C. Brune[15], R.Buchholz[11], L. Büngener[13], J. Bürger[11], F.W. Büsser[13], A. Buniatian[11,39], S. Burke[18], M.J. Burton[22], G. Buschhorn[26], A.J. Campbell[11], T. Carli[26], F. Charles[11], M. Charlet[11], D. Clarke[5], A.B. Clegg[18], B. Clerbaux[4], M. Colombo[8], J.G. Contreras[8], C. Cormack[19], J.A. Coughlan[5], A. Courau[27], Ch. Coutures[9], G. Cozzika[9], L. Criegee[11], D.G. Cussans[5], J. Cvach[30], S. Dagoret[29], J.B. Dainton[19], W.D. Dau[16], K. Daum[34], M. David[9], B. Delcourt[27], L. Del Buono[29], A. De Roeck[11], E.A. De Wolf[4], P. Di Nezza[32], C. Dollfus[37], J.D. Dowell[3], H.B. Dreis[2], A. Droutskoi[24], J. Duboc[29], D. Düllmann[13], O. Dünger[13], H. Duhm[12], J. Ebert[34], T.R. Ebert[19], G. Eckerlin[11], V. Efremenko[24], S. Egli[37], H. Ehrlichmann[35], S. Eichenberger[37], R. Eichler[36], F. Eisele[14], E. Eisenhandler[20], R.J. Ellison[22], E. Elsen[11], M. Erdmann[14], W. Erdmann[36], E. Evrard[4], L. Favart[4], A. Fedotov[24], D. Feeken[13], R. Felst[11], J. Feltesse[9], J. Ferencei[15], F. Ferrarotto[32], K. Flamm[11], M. Fleischer[26], M. Flieser[26], G. Flügge[2], A. Fomenko[25], B. Fominykh[24], M. Forbush[7], J. Formánek[31], J.M. Foster[22], G. Franke[11], E. Fretwurst[12], E. Gabathuler[19], K. Gabathuler[33], J. Garvey[3], J. Gayler[11], M. Gebauer[8], A. Gellrich[11], H. Genzel[1], R. Gerhards[11], A. Glazov[35], U. Goerlach[11], L. Goerlich[6], N. Gogitidze[25], M. Goldberg[29], D. Goldner[8], B. Gonzalez-Pineiro[29], I. Gorelov[24], P. Goritchev[24], C. Grab[36], H. Grässler[2], R. Grässler[2], T. Greenshaw[19], G. Grindhammer[26], A. Gruber[26], C. Gruber[16], J. Haack[35], D. Haidt[11], L. Hajduk[6], O. Hamon[29], M. Hampel[1], M. Hapke[11], W.J. Haynes[5], J. Heatherington[20], G. Heinzelmann[13], R.C.W. Henderson[18], H. Henschel[35], I. Herynek[30], M.F. Hess[26], W. Hildesheim[11], P. Hill[5], K.H. Hiller[35], C.D. Hilton[22], J. Hladký[30], K.C. Hoeger[22], M. Höppner[8], R. Horisberger[33], V.L. Hudgson[3], Ph. Huet[4], M. Hütte[8], H. Hufnagel[14], M. Ibbotson[22], H. Itterbeck[1], M.-A. Jabiol[9], A. Jacholkowska[27], C. Jacobsson[21], M. Jaffre[27], J. Janoth[15], T. Jansen[11], L. Jönsson[21], D.P. Johnson[4], L. Johnson[18], H. Jung[29], P.I.P. Kalmus[20], D. Kant[20], R. Kaschowitz[2], P. Kasselmann[12], U. Kathage[16], J. Katzy[14], H.H. Kaufmann[35], S. Kazarian[11], I.R. Kenyon[3], S. Kermiche[23], C. Keuker[1], C. Kiesling[26], M. Klein[35], C. Kleinwort[13], G. Knies[11], W. Ko[7], T. Köhler[1], J.H. Köhne[26], H. Kolanoski[8], F. Kole[7], S.D. Kolya[22], V. Korbel[11], M. Korn[8], P. Kostka[35], S.K. Kotelnikov[25], T. Krämerkämper[8], M.W. Krasny[6,29], H. Krehbiel[11], D. Krücker[2], U. Krüger[11], U. Krüner-Marquis[11], H. Küster[2], M. Kuhlen[26], T. Kurča[17], J. Kurzhöfer[8], B. Kuznik[34], D. Lacour[29], F. Lamarche[28], R. Lander[7], M.P.J. Landon[20], W. Lange[35], P. Lanius[26], J.-F. Laporte[9], A. Lebedev[25], F. Lehner[11], C. Leverenz[11], S. Levonian[25], Ch. Ley[2], A. Lindner[8], G. Lindström[12], J. Link[7], F. Linsel[11], J. Lipinski[13], B. List[11], G. Lobo[27], P. Loch[27], H. Lohmander[21], J.W. Lomas[22], G.C. Lopez[20], V. Lubimov[24], D. Lüke[8,11], N. Magnussen[34], E. Malinovski[25], S. Mani[7], R. Maraček[17], P. Marage[4], J. Marks[23], R. Marshall[22], J. Martens[34], G. Martin[13], R. Martin[11], H.-U. Martyn[1], J. Martyniak[27], S. Masson[2], T. Mavroidis[20], S.J. Maxfield[19], S.J. McMahon[19], A. Mehta[22], K. Meier[15],

D. Mercer[22], T. Merz[35], A. Meyer[11], C.A. Meyer[37], H. Meyer[34], J. Meyer[11], A. Migliori[28], S. Mikocki[6], D. Milstead[19], F. Moreau[28], J.V. Morris[5], E. Mroczko[6], G. Müller[11], K. Müller[11], P. Murín[17], V. Nagovizin[24], R. Nahnhauer[35], B. Naroska[13], Th. Naumann[35], P.R. Newman[3], D. Newton[18], D. Neyret[29], H.K. Nguyen[29], T.C. Nicholls[3], F. Niebergall[13], C. Niebuhr[11], Ch. Niedzballa[1], R. Nisius[1], G. Nowak[6], G.W. Noyes[5], M. Nyberg-Werther[21], M. Oakden[19], H. Oberlack[26], U. Obrock[8], J.E. Olsson[11], D. Ozerov[24], E. Panaro[11], A. Panitch[4], C. Pascaud[27], G.D. Patel[19], E. Peppel[35], E. Perez[9], J.P. Phillips[22], Ch. Pichler[12], D. Pitzl[36], G. Pope[7], S. Prell[11], R. Prosi[11], K. Rabbertz[1], G. Rädel[11], F. Raupach[1], P. Reimer[30], S. Reinshagen[11], P. Ribarics[26], H.Rick[8], V. Riech[12], J. Riedlberger[36], S. Riess[13], M. Rietz[2], E. Rizvi[20], S.M. Robertson[3], P. Robmann[37], H.E. Roloff[35], R. Roosen[4], K. Rosenbauer[1] A. Rostovtsev[24], F. Rouse[7], C. Royon[9], K. Rüter[26], S. Rusakov[25], K. Rybicki[6], R. Rylko[20], N. Sahlmann[2], D.P.C. Sankey[5], P. Schacht[26], S. Schiek[13], S. Schleif[15], P. Schleper[14], W. von Schlippe[20], D. Schmidt[34], G. Schmidt[13], A. Schöning[11], V. Schröder[11], E. Schuhmann[26], B. Schwab[14], G. Sciacca[35], F. Sefkow[11], M. Seidel[12], R. Sell[11], A. Semenov[24], V. Shekelyan[11], I. Sheviakov[25], L.N. Shtarkov[25], G. Siegmon[16], U. Siewert[16], Y. Sirois[28], I.O. Skillicorn[10], P. Smirnov[25], J.R. Smith[7], V. Solochenko[24], Y. Soloviev[25], J. Spiekermann[8], H. Spitzer[13], R. Starosta[1], M. Steenbock[13], P. Steffen[11], R. Steinberg[2], B. Stella[32], K. Stephens[22], J. Stier[11], J. Stiewe[15], U. Stößlein[35], K. Stolze[35], J. Strachota[30], U. Straumann[37], W. Struczinski[2], J.P. Sutton[3], S. Tapprogge[15], R.E. Taylor[38,27], V. Tchernyshov[24], C. Thiebaux[28], G. Thompson[20], P. Truöl[37], J. Turnau[6], J. Tutas[14], P. Uelkes[2], A. Usik[25], S. Valkár[31], A. Valkárová[31], C. Vallée[23], D. Vandenplas[28], P. Van Esch[4], P. Van Mechelen[4], A. Vartapetian[11,39], Y. Vazdik[25], P. Verrecchia[9], G. Villet[9], K. Wacker[8], A. Wagener[2], M. Wagener[33], A. Walther[8], G. Weber[13], M. Weber[11], D. Wegener[8], A. Wegner[11], H.P. Wellisch[26], L.R. West[3], S. Willard[7], M. Winde[35], G.-G. Winter[11], C. Wittek[13], A.E. Wright[22], E. Wünsch[11], N. Wulff[11], T.P. Yiou[29], J. Žáček[31], D. Zarbock[12], Z. Zhang[27], A. Zhokin[24], M. Zimmer[11], W. Zimmermann[11], F. Zomer[27], K. Zuber[15], and M. zur Nedden[37]

[1] *I. Physikalisches Institut der RWTH, Aachen, Germany*[a]
[2] *III. Physikalisches Institut der RWTH, Aachen, Germany*[a]
[3] *School of Physics and Space Research, University of Birmingham, Birmingham, UK*[b]
[4] *Inter-University Institute for High Energies ULB-VUB, Brussels; Universitaire Instelling Antwerpen, Wilrijk, Belgium*[c]
[5] *Rutherford Appleton Laboratory, Chilton, Didcot, UK*[b]
[6] *Institute for Nuclear Physics, Cracow, Poland*[d]
[7] *Physics Department and IIRPA, University of California, Davis, California, USA*[e]
[8] *Institut für Physik, Universität Dortmund, Dortmund, Germany*[a]
[9] *CEA, DSM/DAPNIA, CE-Saclay, Gif-sur-Yvette, France*
[10] *Department of Physics and Astronomy, University of Glasgow, Glasgow, UK*[b]
[11] *DESY, Hamburg, Germany*[a]
[12] *I. Institut für Experimentalphysik, Universität Hamburg, Hamburg, Germany*[a]
[13] *II. Institut für Experimentalphysik, Universität Hamburg, Hamburg, Germany*[a]
[14] *Physikalisches Institut, Universität Heidelberg, Heidelberg, Germany*[a]
[15] *Institut für Hochenergiephysik, Universität Heidelberg, Heidelberg, Germany*[a]

[16] *Institut für Reine und Angewandte Kernphysik, Universität Kiel, Kiel, Germany*[a]
[17] *Institute of Experimental Physics, Slovak Academy of Sciences, Košice, Slovak Republic*[f]
[18] *School of Physics and Chemistry, University of Lancaster, Lancaster, UK*[b]
[19] *Department of Physics, University of Liverpool, Liverpool, UK*[b]
[20] *Queen Mary and Westfield College, London, UK*[b]
[21] *Physics Department, University of Lund, Lund, Sweden*[g]
[22] *Physics Department, University of Manchester, Manchester, UK*[b]
[23] *CPPM, Université d'Aix-Marseille II, IN2P3-CNRS, Marseille, France*
[24] *Institute for Theoretical and Experimental Physics, Moscow, Russia*
[25] *Lebedev Physical Institute, Moscow, Russia*[f]
[26] *Max-Planck-Institut für Physik, München, Germany*[a]
[27] *LAL, Université de Paris-Sud, IN2P3-CNRS, Orsay, France*
[28] *LPNHE, Ecole Polytechnique, IN2P3-CNRS, Palaiseau, France*
[29] *LPNHE, Universités Paris VI and VII, IN2P3-CNRS, Paris, France*
[30] *Institute of Physics, Czech Academy of Sciences, Praha, Czech Republic*[f,h]
[31] *Nuclear Center, Charles University, Praha, Czech Republic*[f,h]
[32] *INFN Roma and Dipartimento di Fisica, Universita "La Sapienza", Roma, Italy*
[33] *Paul Scherrer Institut, Villigen, Switzerland*
[34] *Fachbereich Physik, Bergische Universität Gesamthochschule Wuppertal, Wuppertal, Germany*[a]
[35] *DESY, Institut für Hochenergiephysik, Zeuthen, Germany*[a]
[36] *Institut für Teilchenphysik, ETH, Zürich, Switzerland*[i]
[37] *Physik-Institut der Universität Zürich, Zürich, Switzerland*[i]
[38] *Stanford Linear Accelerator Center, Stanford California, USA*
[39] *Visitor from Yerevan Phys.Inst., Armenia*

[a] *Supported by the Bundesministerium für Forschung und Technologie, FRG under contract numbers 6AC17P, 6AC47P, 6DO57I, 6HH17P, 6HH27I, 6HD17I, 6HD27I, 6KI17P, 6MP17I, and 6WT87P*
[b] *Supported by the UK Particle Physics and Astronomy Research Council, and formerly by the UK Science and Engineering Research Council*
[c] *Supported by FNRS-NFWO, IISN-IIKW*
[d] *Supported by the Polish State Committee for Scientific Research, grant No. 204209101*
[e] *Supported in part by USDOE grant DE F603 91ER40674*
[f] *Supported by the Deutsche Forschungsgemeinschaft*
[g] *Supported by the Swedish Natural Science Research Council*
[h] *Supported by GA ČR, grant no. 202/93/2423, GA AV ČR, grant no. 19095 and GA UK, grant no. 342*
[i] *Supported by the Swiss National Science Foundation*

1 Introduction

The electron-proton collider HERA has opened new kinematical regions in the study of Deep Inelastic Scattering (DIS): the regions of large four-momentum transfer Q^2 (up to $Q^2 \approx 10^4$ GeV^2) and small Bjorken-x (down to $x \approx 10^{-4}$). It has been suggested that the small x region may be sensitive to new dynamic features of QCD, e.g. [1]. The ZEUS and H1 collaborations have observed [2, 3] that the proton structure function F_2 exhibits a strong rise towards small Bjorken-x. This rise has caused much debate on whether the HERA data are still in a regime where the QCD evolution of the parton densities can be described by the DGLAP (Dokshitzer-Gribov-Lipatov-Altarelli-Parisi) [4] evolution equations, or whether they extend into a new regime where the QCD dynamics is described by the BFKL (Balitsky-Fadin-Kuraev-Lipatov) [5] evolution equation. The BFKL evolution equation is expected to become applicable in the small x region, since it resums all leading $\alpha_s \ln 1/x$ terms in the perturbative expansion, in contrast to the DGLAP equation. Present F_2 measurements do not yet allow to discriminate between BFKL and conventional DGLAP dynamics [6, 7], and are perhaps too inclusive a measure to be a sensitive discriminator. Hadronic final states may give additional information and could be more sensitive to the parton evolution [8, 9, 10]. In this paper we use the H1 detector to study properties of the hadronic final state, namely the transverse energy flow and the production of forward jets, to test the BFKL versus DGLAP hypothesis. Throughout this paper, "forward" refers to the region around the proton direction in the HERA laboratory frame, and transverse quantities are calculated with respect to the proton direction.

For events at low x, hadron production in the region between the current jet and the proton remnant is expected to be sensitive to the effects of the BFKL or DGLAP dynamics. At lowest order the BFKL and DGLAP evolution equations effectively resum the leading logarithmic $\alpha_s \ln 1/x$ or $\alpha_s \ln Q^2$ contributions respectively. In an axial gauge this amounts to a resummation of ladder diagrams of the type shown in Fig. 1. This shows that before a quark is struck by the virtual photon, a cascade of partons may be emitted. The fraction of the proton momentum carried by the emitted partons, x_i, and their transverse momenta, k_{Ti}, are indicated in the figure. In the leading log DGLAP scheme this parton cascade follows a strong ordering in transverse momentum $k^2_{Tn} \gg k^2_{Tn-1} \gg ... \gg k^2_{T1}$, while there is only a soft (kinematical) ordering for the fractional momentum $x_n < x_{n-1} < ... < x_1$. In the BFKL scheme the cascade follows a strong ordering in fractional momentum $x_n \ll x_{n-1} \ll ... \ll x_1$, while there is no ordering in transverse momentum[11]. The transverse momentum follows a kind of random walk in k_T space: the value of k_{Ti} is close to that of k_{Ti-1}, but it can be both larger or smaller [12]. As a consequence, BFKL evolution is expected to produce more transverse energy E_T than DGLAP evolution [13, 14] in the region between the struck quark and the remnant for low x events. Intriguingly, a numerical BFKL calculation of the transverse energy flow [14] came out close to the measurements published by H1 [15], while the DGLAP prediction is too low. In addition, the DGLAP calculation predicts an increase in transverse energy with rising x, while the BFKL calculation predicts the opposite [13]. With increased statistics, the x dependence of this effect can be studied in more detail in this paper.

Another possible signature of the BFKL dynamics is the rate of jets with transverse

momentum $k_{T\rm jet} \approx Q$ and the momentum fraction of the jet, $x_{\rm jet} = E_{\rm jet}/E_p$, large compared with Bjorken-x [9, 10, 16]. Here $E_{\rm jet}$ and E_p are the energies of the jet and the incoming proton respectively. Due to the strong ordering in DGLAP evolution, the condition ${k_{T\rm jet}}^2 \approx Q^2$ suppresses the phase space for jet production. However jet production from BFKL evolution is governed by the ratio $x_{\rm jet}/x$, which is large. Hence the rate of events with a jet satisfying the selection is predicted to be higher for the BFKL than for the DGLAP scenario.

Apart from numerical calculations, predictions for final state observables are also available as Monte Carlo models, based upon QCD phenomenology. In this report we consider two of the currently available Monte Carlo programs: the MEPS (Matrix Elements plus Parton Showers) and CDM (Colour Dipole Model) models. Both provide good descriptions of fixed target DIS and e^+e^-data [17]. The CDM model [18] provides an implementation of the colour dipole model of a chain of independently radiating dipoles formed by emitted gluons [19]. Photon-gluon fusion events are not described by this picture and are added at a rate given by the QCD matrix elements [20]. The CDM description of gluon emission is similar to that of the BFKL evolution, because the gluons emitted by the dipoles do not obey strong ordering in k_T [21]. The CDM does not explicitly make use of the BFKL evolution equation, however. The MEPS model is an option of the LEPTO generator [20] based on DGLAP dynamics. MEPS incorporates the QCD matrix elements up to first order, with additional soft emissions generated by adding leading log parton showers. The emitted partons are strongly ordered in k_T. Both Monte Carlo programs use the Lund string model [22] for hadronizing the partonic final state. The parton density parametrization used here is that of MRSH [23], which results in a good description of the HERA F_2 measurements[2, 3].

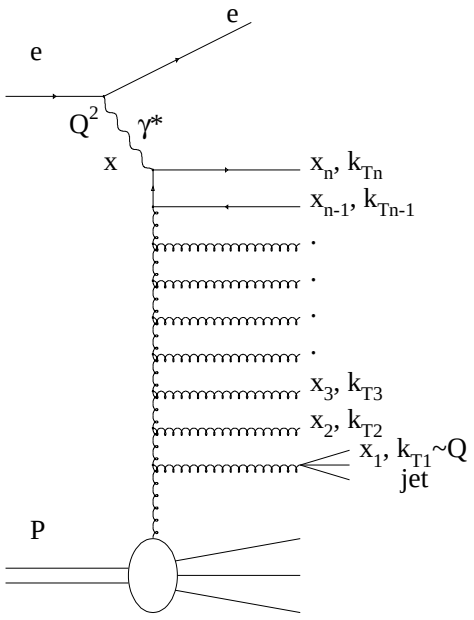

Figure 1: Parton evolution in the ladder approximation. The selection of forward jets in DIS events is illustrated.

2 Detector Description

A detailed description of the H1 apparatus can be found elsewhere [24]. The following briefly describes the components of the detector relevant to this analysis.

The hadronic energy flow and the scattered electrons are measured with a liquid argon (LAr) calorimeter and a backward electromagnetic lead-scintillator calorimeter (BEMC). The LAr calorimeter [25] extends over the polar angular range $4^\circ < \theta < 153^\circ$ with full azimuthal coverage, where θ is defined with respect to the proton beam direction ($+z$ axis). It consists of an electromagnetic section with lead absorbers and a hadronic section with steel absorbers. Both sections are highly segmented in the transverse and longitudinal directions with about 44000 cells in total. The total depth of both calorimeters varies between 4.5 and 8 interaction lengths for $\theta < 125^\circ$. Test beam measurements of the LAr calorimeter modules show an energy resolution of $\sigma_E/E \approx 0.50/\sqrt{E\,[\mathrm{GeV}]} \oplus 0.02$ for charged pions [26]. The hadronic energy measurement is performed by applying a weighting technique in order to account for the non-compensating nature of the calorimeter. The absolute scale of the hadronic energy measurement is presently known to 5%, as determined from studies of the transverse momentum (p_T) balance in DIS events.

The BEMC (depth of 22.5 radiation lengths or 1 interaction length) covers the backward region of the detector, $151^\circ < \theta < 176^\circ$. The BEMC energy scale for electrons is known to an accuracy of 1.7%. Its resolution is given by $\sigma_E/E = 0.10/\sqrt{E\,[\mathrm{GeV}]} \oplus 0.42/E[\mathrm{GeV}] \oplus 0.03$ [27].

The calorimeters are surrounded by a superconducting solenoid which provides a uniform magnetic field of 1.15 T parallel to the beam axis in the tracking region. Charged particle tracks are measured in a central drift chamber and the forward tracking system, covering the polar angular range $7^\circ < \theta < 165^\circ$. A backward proportional chamber (BPC), in front of the BEMC with an angular acceptance of $155.5^\circ < \theta < 174.5^\circ$ serves to identify electrons and to precisely measure their direction. Using information from the BPC, the BEMC and the reconstructed event vertex the polar angle of the scattered electron is known to a precision of 2 mrad.

3 Event Selection and Kinematics

The data used in this analysis were collected in 1993, with electrons of energy $E_e = 26.7$ GeV colliding with protons of energy $E_p = 820$ GeV, resulting in a total centre of mass energy of $\sqrt{s} = 296$ GeV . The data correspond to an integrated luminosity of 320 nb^{-1}. For this analysis DIS events with $Q^2 < 100$ GeV^2 are used, in which the scattered electron is observed in the BEMC. The events are triggered by requiring a cluster of more than 4 GeV in the BEMC. After reconstruction, DIS events are selected in the following way:

- The scattered electron, defined as the most energetic BEMC cluster, must have an energy E'_e larger than 12 GeV and a polar angle θ_e below 173° in order to ensure high trigger efficiency and a small photoproduction background [3].

- The lateral size of the electron cluster, calculated as the energy weighted radial distance of the cells from the cluster centre, has to be smaller than 4 cm. The cluster must be associated with a reconstructed BPC space point which must lie within 4 cm of the cluster centre of gravity. Further reduction of photoproduction background and the removal of events in which an energetic photon is radiated off the incoming electron is achieved by requiring $\sum_j (E_j - p_{z,j}) > 30$ GeV [3], with the sum extending over all particles j (measured calorimetrically) of the event.

- The radial coordinate of the BPC hit must be less than 60 cm, corresponding to an electron angle above 157° with respect to the nominal interaction point, ensuring full containment of the electron shower in the BEMC.

- The z position of the event vertex reconstructed from charged tracks has to be within 30 cm of the average of all collision events.

- The energy in the forward region ($4.4° < \theta < 15°$) has to be larger than 0.5 GeV in order to exclude diffractive-like events with large rapidity gaps in the forward region [28, 15].

The kinematic variables are determined using information from the scattered electron: $Q^2 = 4\, E_e\, E'_e \cos^2(\theta_e/2)$ and $y = 1 - (E'_e/E_e) \cdot \sin^2(\theta_e/2)$. The scaling variable x is then derived via $x = Q^2/(ys)$, and the hadronic invariant mass squared is $W^2 = m_p^2 + sy - Q^2$.

- As the precision of the y measurement degrades with $1/y$, a cut $y > 0.05$ is imposed. Events suffering from QED radiation or from a badly reconstructed electron are removed by requiring that they also fulfil this cut if y is calculated from the measured hadrons.

4 Transverse Energy Flows

The event sample for the energy flow measurements, in which 60% of the total luminosity has been used, contains 9529 DIS events with $5\ \text{GeV}^2 < Q^2 < 100\ \text{GeV}^2$ and with $10^{-4} < x < 10^{-2}$. The measurements are performed in the hadronic centre of mass system (CMS), that is the rest system of the proton and the exchanged boson. The orientation of the CMS is such that the direction of the exchanged boson defines the positive z' axis.

The x – Q^2 plane is divided into three slices with constant Q^2 and varying x, resulting in 9 kinematic bins (see Table 1). In Fig. 2, the flow of transverse energy, as measured with the LAr and BEMC calorimeters, is shown as a function of pseudorapidity $\eta = -\ln\tan(\theta/2)$ for the individual kinematic bins. The data are corrected for detector effects using the CDM generator and a full simulation of the H1 detector response. The data in general exhibit a moderate slope, extending from the current region towards the proton remnant up to the edge of the detector acceptance. For large x and Q^2 the data are reasonably well described by the two models under consideration, MEPS and CDM. At small x and Q^2 however, the models, in particular MEPS, deviate significantly from the data. The MEPS model generates too little E_T. The CDM is able to describe the

x /10^{-3}	Q^2 / GeV^2	$\langle x \rangle$ /10^{-3}	$\langle Q^2 \rangle$/ GeV^2	$\langle E_T \rangle$ (GeV/unit rapidity)	
				measured	BFKL calc.
0.1–0.2	5–10	0.16	6.8	2.12 ± 0.15	1.82
0.2–0.5	6–10	0.30	8.6	2.09 ± 0.12	1.69
0.2–0.5	10–20	0.37	13.1	2.17 ± 0.12	1.77
0.5–0.8	10–20	0.63	14.2	1.95 ± 0.12	1.68
0.8–1.5	10–20	1.1	14.0	1.87 ± 0.11	1.57
1.5–4.0	10–20	2.3	14.5	1.67 ± 0.12	
0.5–1.4	20–50	0.93	28.8	2.12 ± 0.12	
1.4–3.0	20–50	2.1	30.9	1.99 ± 0.13	
3.0–10	20–50	4.9	32.6	1.75 ± 0.17	

Table 1: Values of $\langle E_T \rangle$ measured in the CMS pseudorapidity interval from -0.5 to 0.5 as a function of x and Q^2 . The errors quoted contain the statistical and the systematic point-to-point errors added in quadrature. An overall uncertainty of 9% is not included. Also given are perturbative BFKL predictions calculated according to [14] (see text).

E_T flow towards the remnant, but overestimates the E_T in the current region, around $\eta = 3$. We note that in events where the hard subprocess leads to two hard jets in the detector, both models provide a good description of the energy flow [29] around the jets.

In order to quantify the evolution of E_T with x and Q^2, the average E_T per unit of pseudorapidity is measured in the central pseudorapidity range $-0.5 < \eta < 0.5$. Note that this corresponds roughly to the forward range $2 < \eta_{\rm lab} < 3$ in the laboratory frame. The measured values of $\langle E_T \rangle$ as a function of x are shown for the three Q^2 slices in Fig. 3a, and summarized in Table 1. They are of the order of 2 GeV per unit of pseudorapidity. For $\langle Q^2 \rangle \approx 14$ GeV^2 , the $\langle E_T \rangle$ drops by about 25% when going from $\langle x \rangle = 0.37{\cdot}10^{-3}$ to $2.3{\cdot}10^{-3}$. Though less significant, the data at $\langle Q^2 \rangle \approx 8$ GeV^2 and at $\langle Q^2 \rangle \approx 30$ GeV^2 confirm these $\langle E_T \rangle$ measurements. For fixed x, the level of E_T rises slightly with Q^2 [1].

The errors shown in Fig. 3a are the statistical and systematic point-to-point errors added in quadrature, which are typically 5 % each. The corrections for detector effects are typically 20%. The uncertainty in the BEMC calibration (1.7%) leads to a sizeable effect (4%) in the bin of largest x and Q^2. Small effects from QED radiation (typically 1–2%) and from photoproduction background in the lowest x and Q^2 bin (3%), estimated from Monte Carlo simulations, are not corrected for but absorbed in the systematic error. The model dependence of the correction was investigated with the CDM and MEPS models and leads to a 4% point-to-point error and a 5% overall error. In addition, an overall scale error of 7% arises from the calorimeter calibration (5%), and from varying details of the analysis method, such as the treatment of noise in the calorimeter, clustering of calorimeter cells, and the simulation of the calorimeter response, affecting the result by 5% in the forward region.

Fig. 3a and Table 1 display the prediction for $\langle E_T \rangle$ from a BFKL based QCD calcu-

[1] When W and Q^2 are chosen as kinematic variables, $\langle E_T \rangle$ is found to rise with W and to be almost independent of Q^2 .

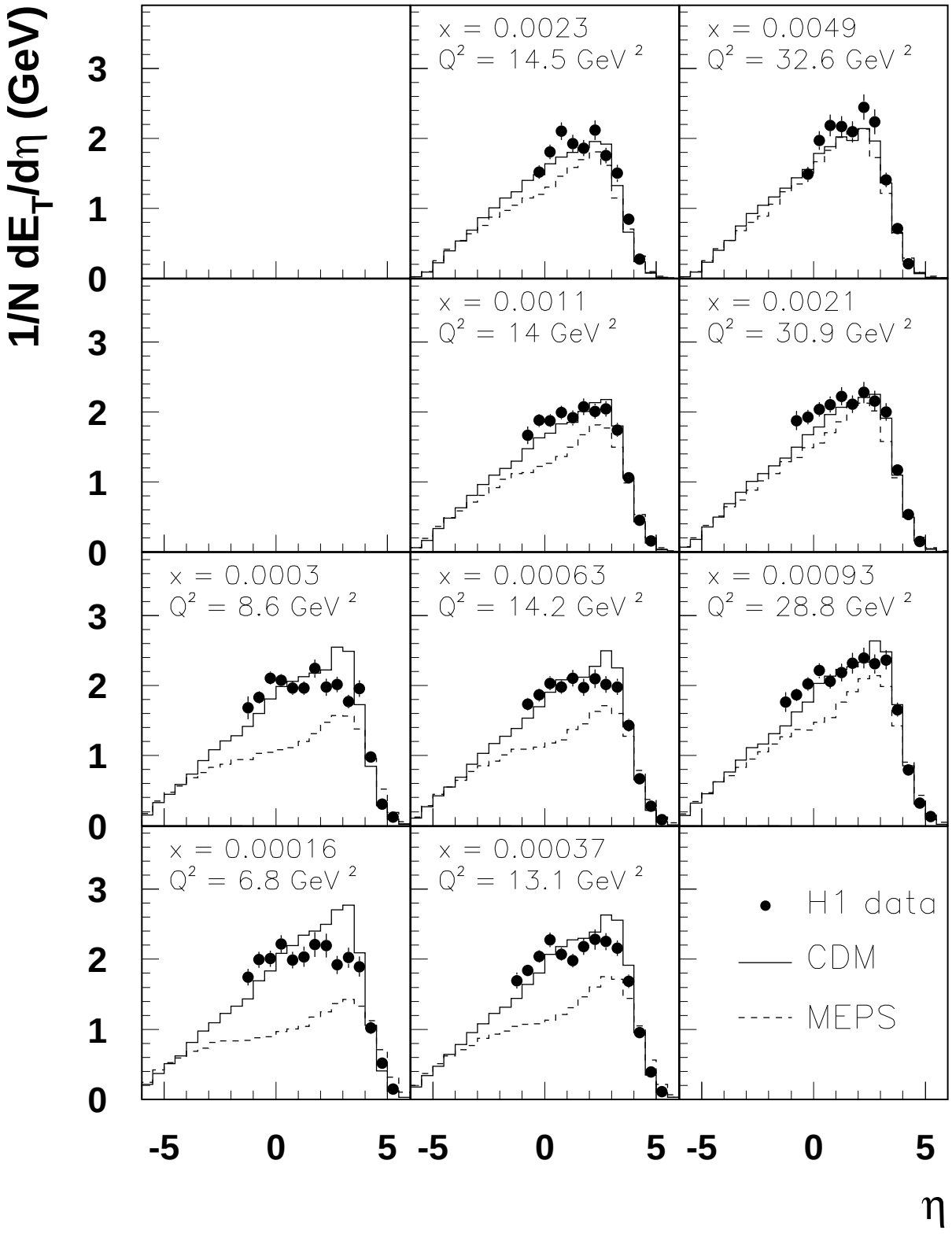

Figure 2: The flow of transverse energy E_T in the CMS as a function of pseudorapidity η. The remnant direction is to the left. Shown are data for nine different kinematic bins (see Table 1). The distributions are normalized to the number of events N in each case. Only statistical errors are shown. For comparison, the models CDM (full line) and MEPS (dashed) are overlayed.

lation [14], yielding values of the order of 1.7 GeV per unit of pseudorapidity and with similar slopes as a function of x as seen in the data. The validity of the calculation [14] is limited to the range shown. A DGLAP based calculation yields an $\langle E_T \rangle$ of around 0.4 GeV [14] with the opposite x dependence. These calculations however do not include the non-perturbative hadronization. This can presently only be included using Monte Carlo models which contain both the perturbative QCD evolution and a phenomenological hadronization model. Since the CDM provides a reasonable description of the data, and since the perturbative BFKL calculation of $\langle E_T \rangle$ is close to the partonic final state $\langle E_T \rangle$ produced perturbatively in the CDM (see Fig. 3a), the CDM may provide an estimate of the effect of hadronization on the BFKL $\langle E_T \rangle$ calculation. That effect can be seen in Fig. 3a, where the $\langle E_T \rangle$ according to the CDM is plotted before and after hadronization. It amounts to an increase in $\langle E_T \rangle$ of 0.3-0.4 GeV and is rather independent of x. When taking into account the hadronization effect as modelled by the CDM, the BFKL calculation is in good agreement with the data. In this context it is interesting to observe that the Monte Carlo model without k_T ordering, the CDM, is consistent with the BFKL calculation for the perturbative part, and that it is able to describe the measured magnitude and x dependence of $\langle E_T \rangle$ reasonably well.

It has to be stressed that the model predictions depend on a variety of parameters which can be tuned [15]. For this analysis the model settings were chosen such as to render a good description of the measured energy flow at large x and Q^2, a kinematic region where theoretical uncertainties are minimal. CDM and MEPS were used in the program implementations ARIADNE 4.03 and LEPTO 6.1, respectively. In the MEPS model, divergences of the matrix element are avoided with a cut-off for parton-parton invariant masses, $m_{ij} > y_{\rm cut} \cdot W$. For this analysis the MEPS cut-off was parametrized such as to follow the limit at which the order α_s contribution exceeds the total cross section within a margin of 2 GeV . For the CDM the standard value of the parameter $y_{\rm cut}$ ($y_{\rm cut} = 0.015$) is used to regulate the admixture of boson-gluon fusion events according to the matrix element. Turning off the boson-gluon fusion admixture, or using the same cut-off prescription as described above has little influence on the CDM predictions.

Improvements to the MEPS model are conceivable, for example with an improved scheme for matching parton showers and matrix elements, by changing the arrangement of color connections, or by changes to the remnant fragmentation which is not well tested at small x. Whether or not such improvements can result in an acceptable description of the energy flows while maintaining a good description of other final state observables can presently not be judged. Therefore the failure of the MEPS model to describe $\langle E_T \rangle$ cannot be unambiguously identified with the fact that its parton shower evolution is based upon the DGLAP evolution. For the same reasons the success of the CDM in this respect, where the parton cascade does not obey strong k_T ordering as in the BFKL evolution, is intriguing but may be fortuitous.

Having identified the average E_T as a sensitive observable to test QCD predictions, it is interesting as well to study the shape of the E_T distribution. The distribution of the observed E_T in the central pseudorapidity bin $-0.5 < \eta < 0.5$ is shown in Fig. 3b for a kinematic bin at low x and Q^2. The CDM gives a reasonable description of the data, and the MEPS model produces events accumulating at lower values of E_T than the majority of the data events. The difference in $\langle E_T \rangle$ between the data and the MEPS model does

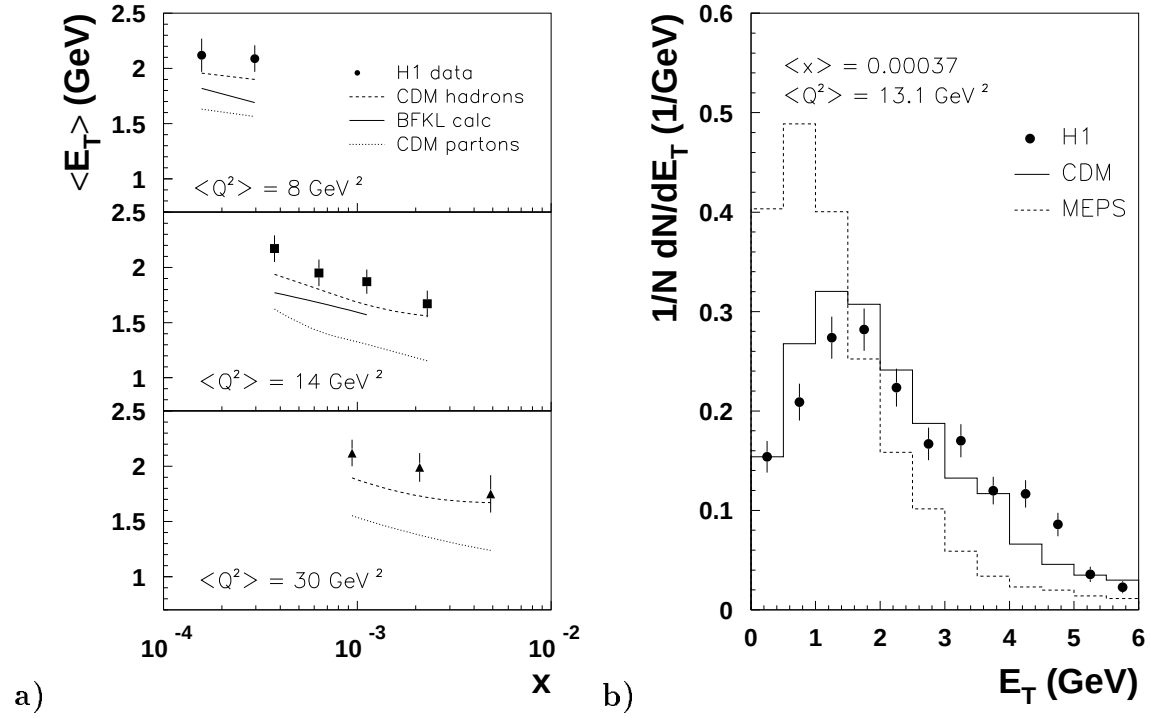

Figure 3: **a)** Transverse energy as a function of x for three different values of Q^2 . The transverse energy $\langle E_T \rangle$ is measured in the CMS in the pseudorapidity range from -0.5 to $+0.5$. Shown are the H1 data, corrected for detector effects, the BFKL calculation and the prediction from the CDM before (partons) and after (hadrons) hadronization. The error bars contain the statistical and the systematic point-to-point errors added in quadrature. An overall scale uncertainty of 9% is not shown. **b)** The uncorrected distribution of the E_T (as defined above) for the events of the kinematic bin with $\langle x \rangle = 0.37 \cdot 10^{-3}$ and $\langle Q^2 \rangle = 13.1$ GeV^2 . The data are compared with the CDM and MEPS models, including a full simulation of the H1 detector.

not seem to stem from a tail in the data.

5 Forward Jets

We have studied DIS events at small x which have a jet with large $x_{\rm jet}$ [30]. A cone algorithm is used to find jets, requiring an E_T larger than 5 GeV in a cone of radius $R = \sqrt{\Delta\eta^2 + \Delta\phi^2} = 1.0$ in the space of pseudo-rapidity η and azimuthal angle ϕ in the HERA frame of reference. In addition to the selections given in section 3, the requirement $y > 0.1$ was imposed to ensure that the jet of the struck quark is well within the central region of the detector and is expected to have a jet angle larger than 60^0. In this sample of DIS events with $Q^2 \approx 20$ GeV^2 and $2 \cdot 10^{-4} < x < 2 \cdot 10^{-3}$ we have counted events which have a "forward" jet defined by $x_{\rm jet} > 0.025$, $0.5 < {p_{T\rm jet}}^2/Q^2 < 4$, $6^0 < \theta_{\rm jet} < 20^0$ and $p_{T\rm jet} > 5$ GeV, where $p_{T\rm jet}$ is the transverse momentum of the jet. A typical event with a high energy forward jet is shown in Fig. 4a. The transverse energy flow around the forward jet axis, averaged over all selected events, is shown versus η and ϕ in Figs. 4b

x range	data events	MEPS events	CDM events	$\sigma(ep \to \text{jet} + X)$ (pb)
$2 \cdot 10^{-4} - 1 \cdot 10^{-3}$	271	141	282	$709 \pm 42 \pm 166$
$1 \cdot 10^{-3} - 2 \cdot 10^{-3}$	158	101	108	$475 \pm 39 \pm 110$

Table 2: Numbers of observed DIS events with a selected forward jet, corrected for radiative events faking this signature. These may be directly compared with the expectations from the Monte Carlo models. The measured cross section $ep \to \text{jet} + X$ for forward jets is also given. The errors reflect the statistical and systematic uncertainties.

and 4c. Distinct jet profiles are observed, which are well described by the Monte Carlo models.

The resulting number of events observed with at least one forward jet in the kinematical region $160^0 < \theta_e < 173^0$ and $E_e > 12$ GeV is given in Table 2 and compared to expectations of the MEPS and CDM models after detector simulation. The data are corrected for photoproduction background and radiative events, which due to the changed kinematics at the hadron vertex can eject a jet in the forward direction. About 4% of the data events were found to contain two forward jets. Results on jet production for both models have been compared with data in previous analyses [31, 32]. In particular the MEPS model was found to show good agreement with the data outside the forward region. In the kinematic range studied here the CDM generally describes the data better than the MEPS model. The predictions were found not to depend significantly on the uncertainties of the proton structure function. However, increasing the x_{jet} cut from 0.025 to 0.05 reduces the total number of events with forward jets to 46 for CDM, to 77 for MEPS and to 105 for the data, hence CDM does not describe the rate of high energy jets.

The measured cross section for forward jets satisfying the cuts given above is also presented in Table 2. It has been corrected for detector effects using the CDM. The systematic errors include effects from DIS event selection, the calorimeter energy scale (5%), the jet angle bias (10 mrad), the proton structure function, and a global normalization uncertainty of 4.5%. Event pile-up effects were found to be negligible. The systematic errors on the two data points are largely correlated. The ratio of the jet cross section for the low x to the high x bin is 1.49 ± 0.25.

The precision of the data does not yet allow a firm conclusion to be drawn. We note, however, that the forward jet cross section is larger in the low x bin than in the high x bin. This is expected from BFKL dynamics as an analytical calculation [10, 33] at the parton level demonstrates: in the kinematical region selected the ratio of the cross sections in the low x bin to high x bin is 1.62 for a calculation including BFKL evolution, compared to 1.03 for a calculation without gluon emission from the ladder in Fig. 1.

6 Conclusions

In order to shed light on the QCD mechanism responsible for parton evolution in the regime of small Bjorken-x, the production of particles and of jets in the forward region has been measured at HERA. A forward jet selection designed to enhance the yield in

electron

forward
jet

BEMC

liquid argon

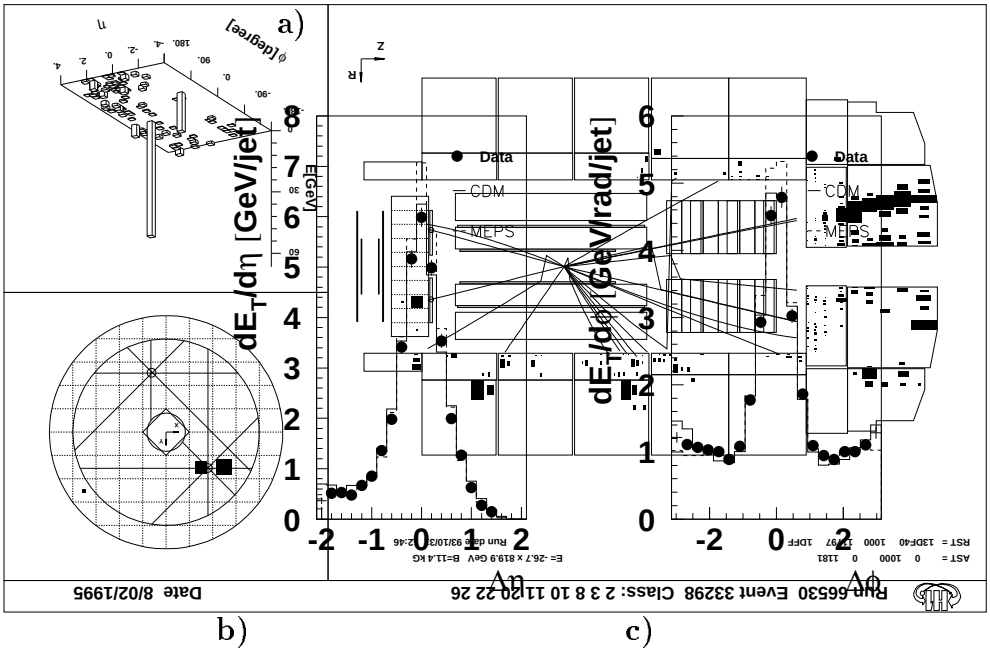

Figure 4: **a)** DIS event event with a forward jet in the H1 detector. The protons are incident from the right, electrons from the left. The scattered electron is detected in the backward electromagnetic calorimeter (BEMC) with an angle of 166^0 and an energy of 18.9 GeV. The forward jet is observed in the liquid argon calorimeter and has an angle $\theta_{\rm jet} = 11^0$ and an energy $E_{\rm jet} = 65$ GeV. Averaged over all events with a selected forward jet, the transverse energy flow around the forward jet axis is shown in **b)** as a function of $\Delta\eta$, integrated over $|\Delta\phi| < 1.0$ and in **c)** as a function of $\Delta\phi$, integrated over $|\Delta\eta| < 1.0$. Here $\Delta\eta$ and $\Delta\phi$ are measured with respect to the reconstructed jet axis.

the case of BFKL evolution, and to suppress the yield for DGLAP evolution, results in a rate of observed forward jets compatible with the BFKL expectation. A firm conclusion on the growth with x however would necessitate a larger data sample.

The flow of transverse energy versus pseudorapity in the hadronic centre of mass system has been measured as a function of the kinematic variables x and Q^2. The observed magnitude and x dependence of the average transverse energy is in agreement with a perturbative QCD calculation based upon the BFKL mechanism, assuming a non-perturbative contribution from hadronization as predicted by the colour dipole model. Though the BFKL mechanism provides a natural explanation of the data, it is also possible that the currently used hadronization scheme is inadequate, and that improved DGLAP based models may also be able to describe the observed features of transverse energy production. The data, which are corrected for detector effects, provide important constraints for further development of the understanding of QCD at small x.

Acknowledgements. We are grateful to the HERA machine group whose outstanding efforts made this experiment possible. We appreciate the immense effort of the engineers and technicians who constructed and maintained the detector. We thank the funding agencies for financial support. We acknowledge the support of the DESY technical staff. We also wish to thank the DESY directorate for the hospitality extended to the non-DESY members of the collaboration. We thank A.D. Martin and P.J. Sutton for repeating the published BFKL calculations for the kinematic bins covered by this analysis, and G. Ingelman for helpful discussions on the Monte Carlo models.

References

[1] J. Bartels and J. Feltesse, Proc. of the Workshop on Physics at HERA, Hamburg 1991, eds. W. Buchmüller and G. Ingelman, vol. 1, p. 131;
E.M. Levin, Proc. QCD – 20 Years Later, Aachen 1992, eds. P.M. Zerwas, H.A. Kastrup, vol. 1, p. 310.

[2] ZEUS Collab., M. Derrick et al., Z. Phys. C65 (1995) 379.

[3] H1 Collab., T. Ahmed et al., Nucl. Phys. B439 (1995) 471.

[4] Yu. L. Dokshitzer, Sov. Phys. JETP 46 (1977) 641;
V.N. Gribov and L.N. Lipatov, Sov. J. Nucl. Phys. 15 (1972) 438 and 675;
G. Altarelli and G. Parisi, Nucl. Phys. 126 (1977) 297.

[5] E.A. Kuraev, L.N. Lipatov and V.S. Fadin, Sov. Phys. JETP 45 (1972) 199;
Y.Y. Balitsky and L.N. Lipatov, Sov. J. Nucl. Phys. 28 (1978) 282.

[6] A.J. Askew, J. Kwieciński, A.D. Martin, P.J. Sutton, Phys. Lett. B325 (1994) 212.

[7] H1 Collab., S. Aid et al., DESY 95-081 (1995).

[8] G. Marchesini, B.R. Webber, Nucl. Phys. B349 (1991) 617.

[9] A.H. Mueller, Nucl. Phys. B (Proc. Suppl.) 18C (1990) 125; J. Phys. G17 (1991) 1443.

[10] J. Kwieciński, A.D. Martin, P.J. Sutton, Phys. Rev. D46 (1992) 921.

[11] A.H. Mueller, Columbia preprint CU-TP-658 (1994).

[12] J. Bartels, H. Lotter, Phys. Lett. B309 (1993) 400.

[13] J. Kwieciński, A.D. Martin, P.J. Sutton and K.Golec-Biernat, Phys. Rev. D50 (1994) 217.

[14] K.Golec-Biernat, J. Kwieciński, A.D. Martin and P.J. Sutton, Phys. Lett. B335 (1994) 220.

[15] H1 Collab., I. Abt et al., Z. Phys. C63 (1994) 377.

[16] J. Bartels, A. De Roeck, M. Loewe, Z. Phys. **C54** (1992) 635;
W.K. Tang, Phys. Lett. B278 (1992) 363.

[17] EMC Collab., M. Arneodo et al., Z. Phys. C36 (1987) 527;
OPAL Collab., M.Z. Akrawy et al., Z. Phys. C47 (1990) 505;
N. Magnussen et al., Proc. of the Workshop on Physics at HERA, Hamburg 1991, eds. W. Buchmüller and G. Ingelman, vol. 3, p. 1167.

[18] L. Lönnblad, Computer Phys. Comm. 71 (1992) 15.

[19] G. Gustafson, Ulf Petterson, Nucl. Phys. B306 (1988);
G. Gustafson, Phys. Lett. B175 (1986) 453;
B. Andersson, G. Gustafson, L. Lönnblad, Ulf Petterson, Z. Phys. C43 (1989) 625.

[20] G. Ingelman, Proc. of the Workshop on Physics at HERA, Hamburg 1991, eds. W. Buchmüller and G. Ingelman, vol. 3, p. 1366.

[21] L. Lönnblad, Z. Phys. C65 (1995) 285;
A. H. Mueller, Nucl. Phys. B415 (1994) 373;
L. Lönnblad, CERN-TH/95-95.

[22] T. Sjöstrand, Comp. Phys. Comm. 39 (1986) 347;
T. Sjöstrand and M. Bengtsson, Comp. Phys. Comm. 43 (1987) 367;
T. Sjöstrand, CERN-TH-6488-92 (1992).

[23] A.D. Martin, W.J. Stirling and R.G. Roberts, Proc. of the Workshop on Quantum Field Theory and Theoretical Aspects of High Energy Physics, eds. B. Geyer and E.M. Ilgenfritz (1993) p. 11.

[24] H1 Collab., I. Abt et al., DESY 93-103 (1993).

[25] H1 Calorimeter Group, B. Andrieu et al., Nucl. Instr. and Meth. A336 (1993) 460.

[26] H1 Calorimeter Group, B. Andrieu et al., Nucl. Instr. and Meth. A336 (1993) 499.

[27] H1 Collab., I. Abt et al., Nucl. Phys. B407 (1993) 515.

[28] ZEUS Collab., M. Derrick et al., Phys. Lett. B315 (1993) 481;
H1 Collab., T. Ahmed et al., Nucl.Phys. B429 (1994) 477.

[29] H1 Collab., S. Aid et al., DESY 95-086 (1995).

[30] J. Kurzhöfer, Ph.D. thesis, Universität Dortmund (1995).

[31] H1 Collaboration, T. Ahmed et al., Phys. Lett. B346 (1995) 415.

[32] H1 Collaboration, I. Abt et al., Z. Phys. C61 (1994) 59.

[33] V. Del Duca, talk at the Workshop on Deep Inelastic Scattering and QCD, Paris 1995 (to appear in the proceedings); M. Wüsthoff, private communication.